HyperProbe

Project title: Transforming brain surgery by advancing functional-guided neuronavigational imaging

Project acronym: HyperProbe

Grant Agreement: 101071040

Call identifier: HORIZON-EIC-2021-PATHFINDERCHALLENGES-01

D3.2 Simple liquid phantom delivery

Lead partner:	UCL
Author(s):	Frédéric Lange (UCL), Angelos Artemiou (UCL), Luca Giannoni (UNIFI), Anam Toaha (UNIFI), Ilias Tachtsidis (UCL)
Work Package:	WP3
Due date:	Month 24
Actual delivery date:	30/09/2024
Type:	DATA
Dissemination level:	PU

Funded by the European Union

European Innovation Council

Tables of contents

Abbreviations

CCO	Cytochrome-c-oxidase
ETC	Electron transport chain
DO_2	Dissolved oxygen
FAD	Flavin adenine dinucleotide
FOV	Field of view
HHb	Deoxyhaemoglobin
HbO_2	Oxyhaemoglobin
IL	Intralipid
NAD	Nicotinamide adenine dinucleotide
NIR	Near-infrared
NIRS	Near-infrared spectroscopy
N_2	Nitrogen
O_2	Oxygen
PBS	Phosphate-buffered saline
PpIX	Protoporphyrin IX
SNR	Signal-to-noise ratio
WP	Work Package

Disclaimer

1. Introduction

This deliverable presents the development of simple liquid phantom recipes that can be replicated by all the partners to enable the validation of the accuracy of the measurements of the various iteration of the developed HyperProbe prototypes, as well as their capabilities to target specific optical contrasts and biomarker signatures (detailed in section 2.2).

In particular, we will present two types of liquid phantoms that have been developed to assess different aspects of the HyperProbe systems. The first type has been designed to assess the basic instrument capabilities in terms of signal-to-noise ratio (SNR) and dynamic range, in response to changes in the optical properties of the tissues (i.e., absorption μ_a and reduced scattering μ'_s). The second type of phantom has been developed to assess the capacity of the systems to detect specific biochemical contrasts of interest.

In this report, we will firstly describe the rationale of the phantoms developed here and the specifics goals that we want to achieve with them. Then, we will describe the recipes for the evaluation of the basic instrument capabilities and the one developed to be used to test the capacity of the HyperProbe system to target specific contrasts.

2. Phantom development

2.1. General considerations on optical liquid phantom developments to mimic biological tissues.

The development of novel optical methods or instruments aiming at probing biological tissues requires the uses of tissue-simulating objects as to mimic their properties[1], so the new instruments and/or methods can be rigorously validated.

In diffuse optics, the two main properties studied are the absorption and the reduced scattering parameters[2]. In particular, the absorption spectrum is linked to the biochemistry of the tissues through the main constituents that absorb light in the spectral range of interest. Conversely, the scattering spectrum is linked to the fine structure of the tissue. Therefore, in order to assess the accuracy of novel instruments and methods, one needs to produce phantoms with calibrated absorption and scattering properties.

To do so, one could use either solid or liquid phantoms. Both types of phantoms present their owns sets of characteristics, advantages and drawbacks[1]. The main advantage of solid phantom is that they are robust, meaning that they last in time, and can be transported easily to compare various systems. However, the main disadvantage of these phantoms is that the absorption and scattering properties can't replicate the exact spectral shape of tissues' ones over a large bandwidth. On the contrary, liquid phantoms are bulkier and are single use (i.e., lifetime of less than a few hours), but have the advantage of being capable of precisely mimicking the tissues optical properties by using the same compounds as the *in vivo* one (i.e., using real haemoglobin, see section 2.2.A for details).

Therefore, in order to precisely characterise and compare the various iterations of the HyperProbe instruments, we have designed liquid phantom recipes that will be able to mimic exactly the type of contrast that the HyperProbe project is focusing on (see next section for details), thus aiming at testing the accuracy of their detection capabilities.

In the next section, we will detail what specific *in vivo* contrasts we aim to reproduce in our phantom recipes, and the agents that we will use to mimic them in the phantoms.

2.2 Optical contrasts of interest for the HyperProbe project

The HyperProbe project aims at probing the exposed cerebral cortex during neurosurgery to identify, map and quantify healthy functional tissues and differentiate them from tumoral ones. To do so, we will focus on specific contrasts that will enable to distinguish between healthy and tumoral regions of the brain. Below, we will list the main contrasts of interest for the HyperProbe project, and the compounds that will be used in our phantom recipes to mimic them. It is worth noting that we aim to develop an instrument able to perform both reflectance and fluorescence measurements. Therefore, our liquid phantoms will have to be able to produce contrasts for these two types of optical measurements. We will detail below what types of reflectance and fluorescence contrasts we are aiming to identify and reproduce in our liquid phantoms.

A - Reflectance based contrast

Oxygenation

The main contrast that is assessed by optical techniques based on reflectance measurement is the oxygenation of tissues. Indeed, one of the main absorbers in the range 400-1000 nm is haemoglobin, in both its oxygenated (oxyhaemoglobin, HbO_2) and deoxygenated (deoxyhaemoglobin, HHb) forms[2]. As HbO_2 and HHb have different absorption spectra, by performing a measurement at several wavelengths, one can calculate the concentration of each species and infer the corresponding tissue oxygenation levels[3]. The typical absorption spectra of HbO_2 and HHb can be found on figure 1. As the oxygenation values will change as function of the oxygen supply and demand of the tissues, it can thus be used as a biomarker of some aspects of the physiology of the tissue and its status (i.e., tumoral vs. healthy, functional vs. non-functional)[4,5].

In order to mimic this contrast, the advantage in the use of liquid phantoms is the capability to employ actual blood to recreate the exact same absorption properties as in the tissues. Blood liquid phantoms have been widely used in the community to assess the capacity of near-infrared spectroscopy (NIRS) instruments to derive accurate oxygenation values[6,7]. Indeed, by bubbling gas into the phantom, one can either oxygenate (i.e., with Oxygen (O_2)) or deoxygenate (i.e. with nitrogen (N_2)) the phantom, in order to control the oxygenation state of the blood, which provides a way to mimic specific oxygenation states of the tissues. We will use the same process in our phantom to produce the oxygenation contrast.

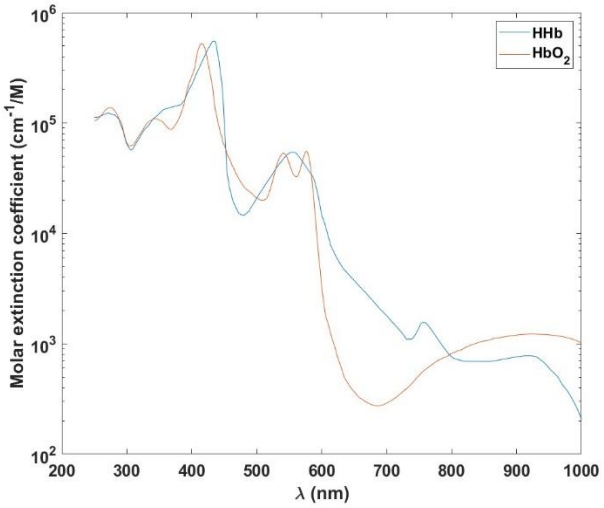

Figure 1. Extinction coefficient of HHb and HbO_2. Spectra extracted from: https://github.com/multimodalspectroscopy/UCL-NIR-Spectra.

Metabolism

Another important contrast that reflectance-based system can monitor is the cellular metabolic activity, via the monitoring of the cytochrome-c-oxidase (CCO), an enzyme in the mitochondria[8]. Coupled with the oxygenation contrast, the metabolic contrast can give a clearer picture about the oxygen consumption of the tissues, which is tightly linked to its status (i.e., tumoral vs. healthy, functional vs. non-functional) [5,9]. This technique has been used specifically to non-invasively monitor brain oxygenation and metabolic status via NIRS[8]. Moreover, on top of the CCO, it is known that other cytochromes species (i.e., cytochrome b and cytochrome c), that appear at various stages of the electron transport chain, have specific absorption spectra, especially in the visible range[8]. These are usually left out of the analysis of the NIRS measurements, as the predominant absorber in the NIR is the CCO. However, as the HyperProbe system is targeting the exposed cortex, and will also cover the visible window, assessing these extra compounds might be feasible. Therefore, we will aim to target them as well. Figure 2 reports the typical absorption spectra of the cytochromes, both for their absolute oxidised and reduced form, and for the oxidized-reduced form, which are typically used to detect cytochrome contrast *invivo*[8].

In order to mimic these contrasts in liquid phantoms, one can use commercial dried yeast[10]. Indeed, yeast presents the same respiratory transport chain that contains cytochromes as in the mitochondria of a human cell. Therefore, commercial dried yeast will be incorporated in our phantoms to reproduce metabolic contrast.

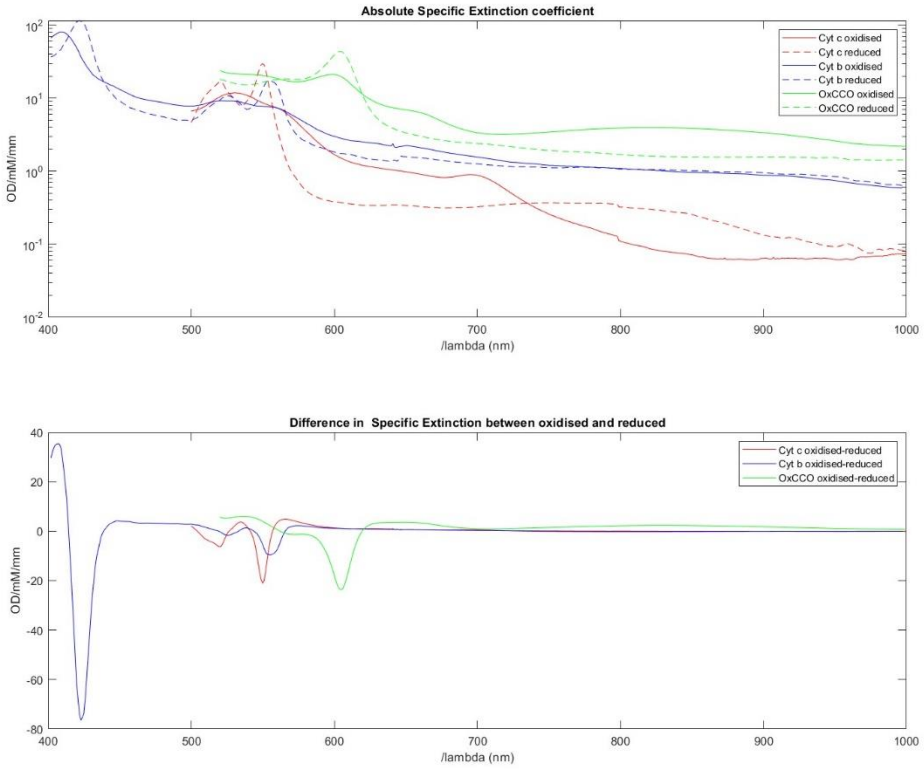

Figure 2. Cytochromes extinction coefficient spectra. Top - absolute oxidised and reduced form, Bottom – oxidised-reduced form. One can note the clear peaks in the visible for the difference in oxidised-spectra form. Spectra extracted from: https://github.com/multimodalspectroscopy/UCL-NIR-Spectra.

Scattering

The scattering properties of the tissues are inherent properties that are determined by their organizations, structures and refractive indexes. Therefore, these properties need to be considered in our modelling to interpret the reflectance spectra. Moreover, the scattering properties can also be used as a biomarker of various tissues type, as they are linked to the tissue's structure. For example, it has been used in NIRS measurements to identify different breast tissues in the context of breast cancer identification[11].

The most common way to induce scattering is to use a solution based on Intralipid, a pharmaceutical product used for parenteral nutrition of patients[12]. It consists of small fat droplets suspended in water that make it a highly scattering medium. We will use Intralipid 20% to calibrate the scattering coefficient of our liquid phantoms (see section 3.1 for typical scattering spectra).

Baseline tissue composition

The two other main absorbers that affect the reflectance spectra of the tissues are water and fat, that both have distinctive spectra in our spectral range of interest[2]. If one wants to assess the absolute absorption spectra of the tissues and perform quantification, these two species need to be considered. Moreover, it has been shown that the quantification of these compounds can help in identifying tissue types by refining the information about their composition. Their identification has notably been used in the context of breasts cancer screening[13]. Therefore, these two compounds will also be of great interest for HyperProbe.

As all the liquid phantoms are water based, the water contrast is inherently present. Moreover, the Intralipid solution used to provide the scattering consists of small fat droplets, thus it can also be used to mimic the fat contribution to the reflectance spectra. Figure 3 shows typical absorption spectra of pure water and fat.

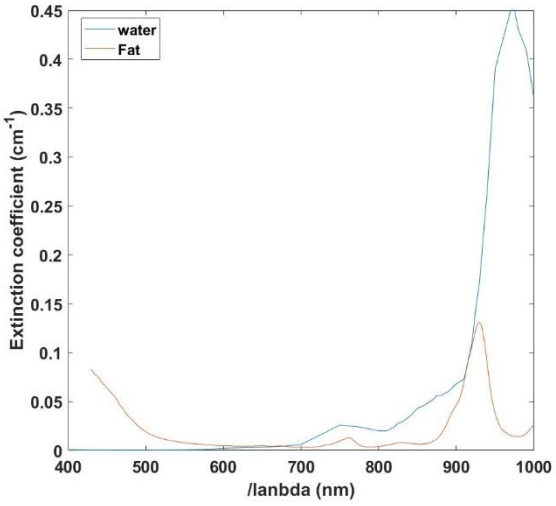

Figure 3. Extinction Coefficient of Water and fat. Spectra extracted from: https://omlc.org/spectra/.

B - Fluorescence based contrast

Fluorescence protoporphyrin IX

One of the main fluorescence measurements of interest in the context of glioma surgery is the 5-aminolevulonic acid (5-ALA)-induced protoporphyrin IX (PpIX) fluorescence that offers the possibility to visualize tumour cells during neurosurgery[14]. PpIX takes part in the biosynthesis of hem and thus naturally occurs in human bodies. During the surgery, the ingestion of 5-ALA, precursor in hem's biosynthesis, leads to temporary enhancement of PpIX concentration in

glioma cells (glioma being tumours)[15]. This fluorescence has been used over the last 20 years as an intraoperative tool to assist neurosurgeons during glioma resection through the use of fluorescence microscopes[16]. Therefore, we aim to incorporate the capability of detecting PPIX fluorescence into our HyperProbe system.

In order to mimic this contrast, the simplest way is to directly add PpIX to our basic blood/lipid liquid phantom[17].

Autofluorescence of flavoproteins and NADH

Flavoproteins (FAD/$FADH_2$) and NADH represent the most targeted intrinsic fluorophores of mitochondrial metabolism in the tissues, due to their autofluorescence properties. The reduced form of NADH shows maximum light absorption in the range 320–380 nm, peaking at 365 nm, and it emits fluorescent light between 420 and 480 nm, with a maximum centred at 450 nm. Since its oxidized form, NAD (also known as NAD+), provides a negligible contribution to light absorption in the above range, it is possible to selectively excite NADH with UV light and detect its fluorescent emission. Variations in the intensity levels of the detected fluorescence indicate changes in the concentration of the reduced state NADH associated with the rate of production of ATP in the neuronal mitochondria. A reduction in the detected fluorescent emission is typically linked to a decrease in the concentration of NADH due to its oxidation in the electron transport chain (ETC), after cerebral metabolic activation that leads to higher energy demand by the brain. It has been demonstrated that the contribution to the fluorescence signal of mitochondrial NADH is 6–8 times greater than that of NADH in cytoplasm, thus connecting NADH fluorescence directly to the process of ATP synthesis[18].

Similar to NADH, $FADH_2$ is also actively involved in mitochondrial energetics as an electron donor in the ETC. However, it is its oxidized form, FAD, that exhibits fluorescence properties with emission in the range 500–560 nm, peaking at around 520 nm, while its absorption spectrum reveals two prominent bands for excitation: one between 320 and 390 nm, the other between 430 and 500 nm (the latter is the most exploited). The response of FAD fluorescence emission to functional activation has been demonstrated to be biphasic: a brief (1–2 s) increase in fluorescence intensity (light phase), corresponding to the onset of the stimulus, is generally followed by a much slower decrease in detected light (dark phase) within a few seconds after the termination of the stimulus[18].

Having access to these contrasts would be a nice addition to our HyperProbe system. However, our current system does not provide illumination in the UV. Nevertheless, we could consider adding this possibility in the future and thus would need compounds to mimic these contrasts in our liquid phantoms. Yeast is a good candidate to also induce these contrasts[19], on top of the standard metabolic one. We will explore this possibility in section 3.2.D.

C – Summary of the contrasts of interest

The ultimate goal of the phantom recipes developed here is to provide means to assess the accuracy of the detection of the optical contrast measured by the HyperProbe systems. Therefore, the development of these recipes needs to be focused on the contrast of interest for our specific application. We have thus listed above the contrasts of interest that we aim to target with the HyperProbe systems, and explained how we can mimic this *in vivo* contrast with specific compounds. Table 1 summarizes the *in vivo* contrast of interest that needs to be modelled by the phantom recipes and the compounds used to mimic them.

*Table 1. Summary of the optical contrast of interest that needs to be modelled by the phantom recipes. *This contrast is not currently targeted by our system but we will explore the possibility to do so in the future.*

Measurement Mode	Signature	In-vivo marker	Mimicking compound	Contrast induced
Reflectance	Oxygenation	Haemoglobins Concentration	Red Blood Cells	Changes in oxygenation by bubbling gas (O_2/N_2)
Reflectance	Metabolism	Cytochrome c, b, oxCCO redox state concentrations	Yeast	Changes in redox state of cytochromes by bubbling O_2
Reflectance	Scattering	Scattering coefficient	Intralipid 20%	Change concentration of Intralipid 20%
Reflectance	Baseline tissue composition	Water and fat content	Water and Intralipid 20%	Change concentration of Intralipid 20%
Fluorescence	PpIX fluorescence	5-ALA induced PpIX	PpIX sigma	Change concentration of PpIX
Fluorescence	Autofluorescence*	FAD and NADH concentrations	Yeast	Changes in redox states of FAD and NADH by bubbling O_2

2.3 Challenges of the detection of the optical contrasts

There are two main challenges in the accurate detection of optical contrast. The first one is the ability to disentangle the absorption and the scattering properties of the tissues. This is addressed by accurate modelling of the light transport in tissues[20], and does not affect the design of the phantoms. The second challenge to detect accurately optical contrast is the potential crosstalk between the different contrasts, i.e., the phenomena that a genuine change in one contrast is also inducing a spurious measured change in another one. Therefore, we need to design phantom recipes that can provide ways to test the absence of crosstalk in the measurements. This is done by having various recipes that can induces changes in one contrast, without affecting the other ones. A common example is the crosstalk between the oxygenation and the metabolic contrasts[8]. To validate the measurements, we need to design phantoms that can induce an oxygenation change without a metabolic change. We will present these strategies in section 3.2.

As we also want to develop phantoms able to test both reflectance and fluorescence measurements, we also need to verify that there will be no interaction or crosstalk between the fluorescence and reflectance measurements. To do so, we will characterize the raw optical properties of the PpIX that we will use as the main fluorescence agent of interest and then run specific characterization experiments to validate the absence of crosstalk between the reflectance and fluorescence measurements (see section 3.2).

3. Phantom recipes

3.1. Phantom recipes for basic instrument characterization

Two different recipes for optical phantoms were produced to assess the basic instrument capabilities in terms of SNR and dynamic range, in response to changes in the optical properties of the mimicked tissues (i.e. absorption μ_a and reduced scattering μ'_s), as well as to characterize the sensitivity of the system as function of such properties. Thus, the results of the testing on such phantoms with all our systems can give us the dynamic range of optical properties that we can cover, and the SNR that we can expect for each selected level of

absorption. To prepare these recipes, two main compounds were selected to introduce absorption and scattering in the phantoms. Indian ink was selected as the main absorber while intralipid 20% was selected for the scattering. The description of these two compounds can be found bellow.

Indian Ink

Indian Ink is a common and inexpensive dye used in liquid phantoms to replicate continuous, broad absorption spectra in a controllable and easily reproducible way, similar to the typical absorption features of known tissue chromophores, e.g., haemoglobin[21]. For this reason, such dye has been selected for the recipe of the liquid phantoms used to test sensitivity of the HyperProbe systems.

The absorption properties of the specific brand of Indian Ink used in our phantoms (Winsor & Newton, Black Indian 951) were directly measured using a commercial spectrophotometer (PerkinElmer LAMBDA 950) located at the UNIFI partner's facilities. The LAMBDA 950 works in transmittance mode and allow to directly estimate the absorption coefficients from the absorbance of a water-based liquid solution (calibrated for the reference with only water) between 400 and 900 nm with 0.5-nm resolution. Therefore, the Indian Ink was diluted in water at different concentrations (0.2, 0.3, 0.4, 0.5 and 0.6 µl/ml) corresponding to values found in literature giving a range of absorption properties equivalent to biological soft. The results of the absorbance curves measured with the LAMBDA 950 are reported in figure 4.

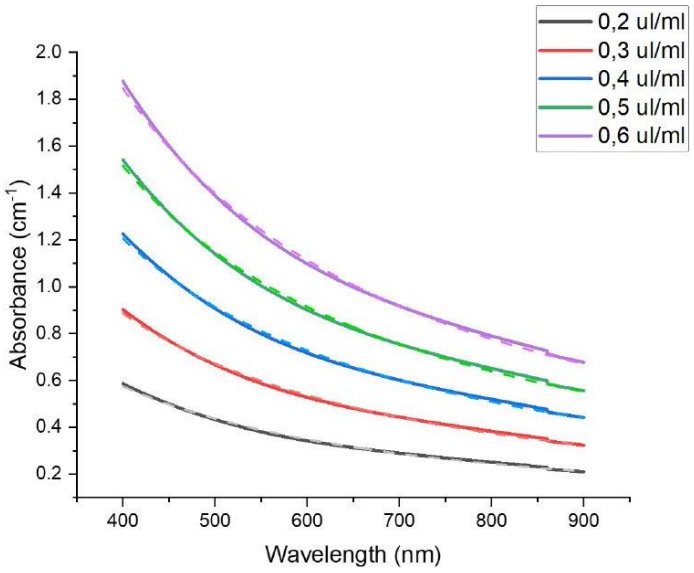

Figure 4. Absorbance curves of Indian Ink experimentally measured with a commercial spectrophotometer at different dilutions in water (solid lines). The dashed lines report the exponential decay fits applied to the curves.

From the experimental absorbance curves obtain with the LAMBDA 950, exponential decay fits were applied on the datasets (as seen in Fig. 4), in order to characterise the theoretical absorption properties of the Indian ink for generalisation to any given concentration. The exponential decay function was defined as $\mu_a = a\lambda^{-b}$ and the results of the fits for the parameters *a* and *b* are reported in Table 2.

Table 2. Results of the exponential decay fits on the experimental curves of Indian Ink, including corresponding R2 coefficients of determination

Concentration (µl/ml)	*a* (cm^{-1}*nm^{-1})	*b*	R^2
0.2	929 ± 17	1.233 ± 0.003	0.997
0.3	1500 ± 24	1.241 ± 0.003	0.998
0.4	2080 ± 32	1.244 ± 0.002	0.998
0.5	2650 ± 39	1.246 ± 0.003	0.998
0.6	3297 ± 46	1.250 ± 0.003	0.999

Intralipid

Intralipid is the most common compounds to induce scattering in liquid phantom[22]. It has been extremely well characterized and had been shown to be a reproducible way. The typical scattering spectra of the Intralipid 20% can be found on figure 5. Thus, from this original pure scattering spectra, one can adjust the scattering properties of the phantoms by appropriate dilution.

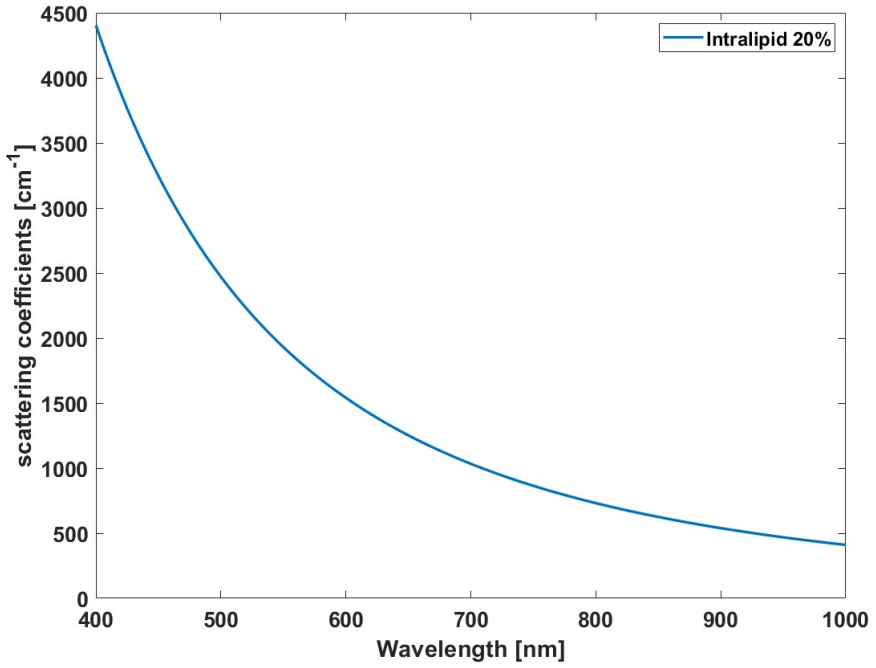

Figure 5. Scattering spectra of Intralipid 20%.

Recipes summary

Table 3 reports the recipe of the two phantoms, the first made of water and Indian ink at different dilutions (named *Phantom W+INK*), whilst the second including also Intralipid 20% to simulate tissue scattering (named *Phantom W+INK+IL*). Phantom W+INK, being a very low scattering and variable absorption (from low to high) recipe, is used to simulate an extreme low-reflectance scenario, with very little light coming back to the imaging system for detection; hence it has the goal of testing the limits in SNR of our systems. On the other hand, Phantom W+INK+IL, simulates a typical basic phantom with tissue-like scattering and variable absorption (from low to high), so its goal is to characterise the sensitivity of our systems to the smallest changes in optical properties of the medium.

Table 3.Recipes of the two basic phantoms used for sensitivity, SNR and dynamic range testing of our HyperProbe systems.

Phantom name	Phantom recipe	Volume of water (mL)	Volume of India ink (μL)	Volume of Intralipid (20%) (mL)
Phantom W+INK	Water; Indian ink	300	From 0 to 9 at steps of 0.5	0
Phantom W+INK+IL	Water; Indian ink; Intralipid (20%)	280	From 0 to 10 at steps of 0.5	20

A – Metrological characterisation of HyperProbe1.1 with basic phantoms

Both phantom recipes in Table 3 have been so far applied to our HyperProbe1.1 system (as described and characterised in Deliverable D1.2), to provide a preliminary metrological characterisation of the setup. Figure 6 depicts the configuration by which HyperProbe1.1 was used to image the phantoms.

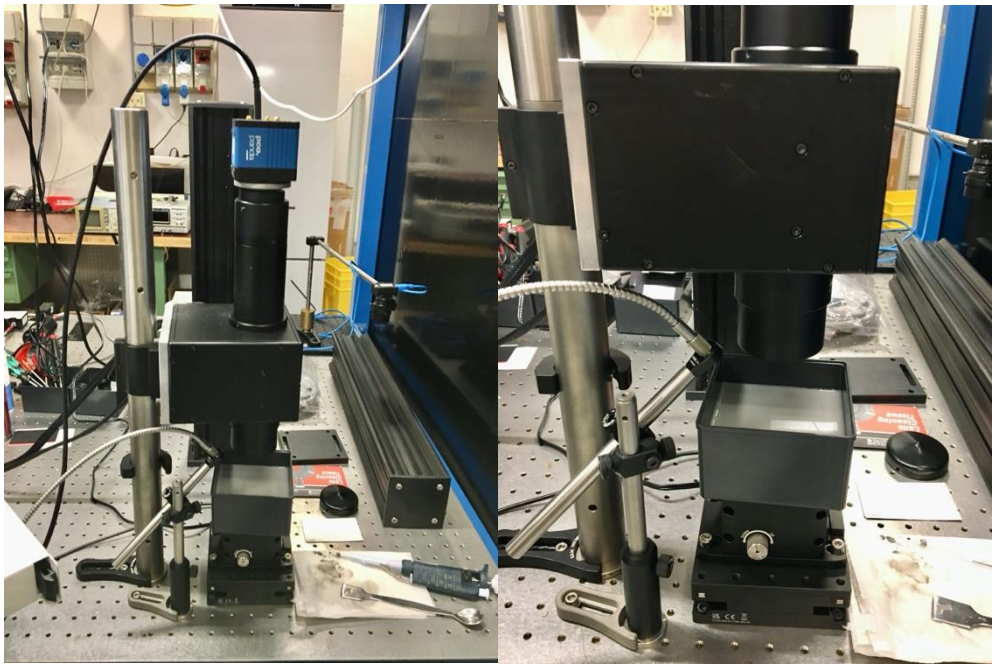

Figure 6.Application of HyperProbe1.1 to the phantoms for basic instrument characterisation.

Characterisation of HyperProbe1.1 with Phantom W+INK

We first imaged reflectance in the working range of the HyperProbe1.1 system (385 to 1015 nm at 5-nm sampling for a total of 127 spectral bands) for a reference phantom containing only water (300mL) with an exposure time of the camera equal to 350 ms. This correspond to the maximum exposure time that can be set to the system according to its calibration (as referenced in Deliverable D1.2). We then sequentially introduced India ink (Winsor & Newton, Black Indian 951) in volumes ranging from 0.5 to 9.0μL, with increments of 0.5μL, into the initial solution of water. For each step, reflected intensity hypercubes were acquired. These hypercubes were then corrected for dark subtraction and normalised for white standard calibration (for details of the procedure, see deliverable D1.2), as to compute the reflectance and the attenuation spectra of the various phantoms' iterations after averaging over the whole field of view (FOV) of 2048 x 2048 pixels (since the phantoms are homogenous and present no spatial features of interest). Average attenuation spectra A were determined from the

formula A= -log$_{10}$(R), where R are the average reflectance spectra. All the resulting attenuation spectra from Phantom W+INK are reported in Figure 7a, whilst Figure 7b depicts the theoretical absorption coefficient of pure water (at the corresponding volumetric fraction) and of the various iteration of the phantom. For Indian ink contribution, these were derived using the formula outlined in section 3.1.

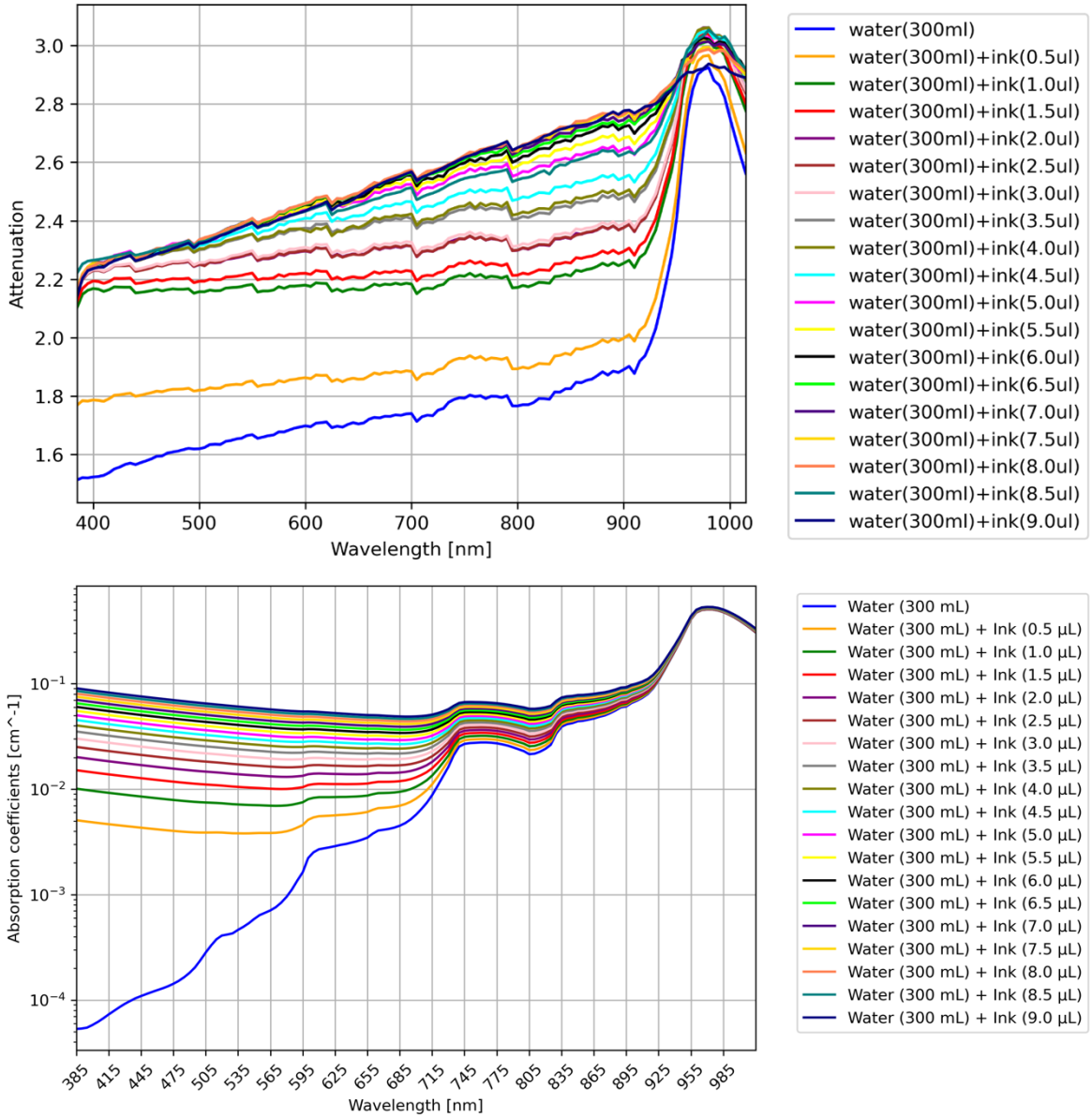

Figure 7.(a) Experimental attenuation spectra of the Phantom W+INK at its various iterations collected and processed from HyperProbe1.1; (b) Theoretical absorption properties of the Phantom W+INK at its various iterations.

The comparison between the reconstructed attenuation from the experimental data collected with HyperProbe1.1 and the theoretical benchmark demonstrates the capability of the system to reproduce the expect trends and shapes of the spectra, despite the low SNR. Differences in attenuation between the various iteration of the Phantom W+INK and the reference phantom containing only water were also calculated in terms of delta of attenuation (Δ attenuation) across all the different wavelengths from 385 to 1015 nm., as depicted in Figure 8.

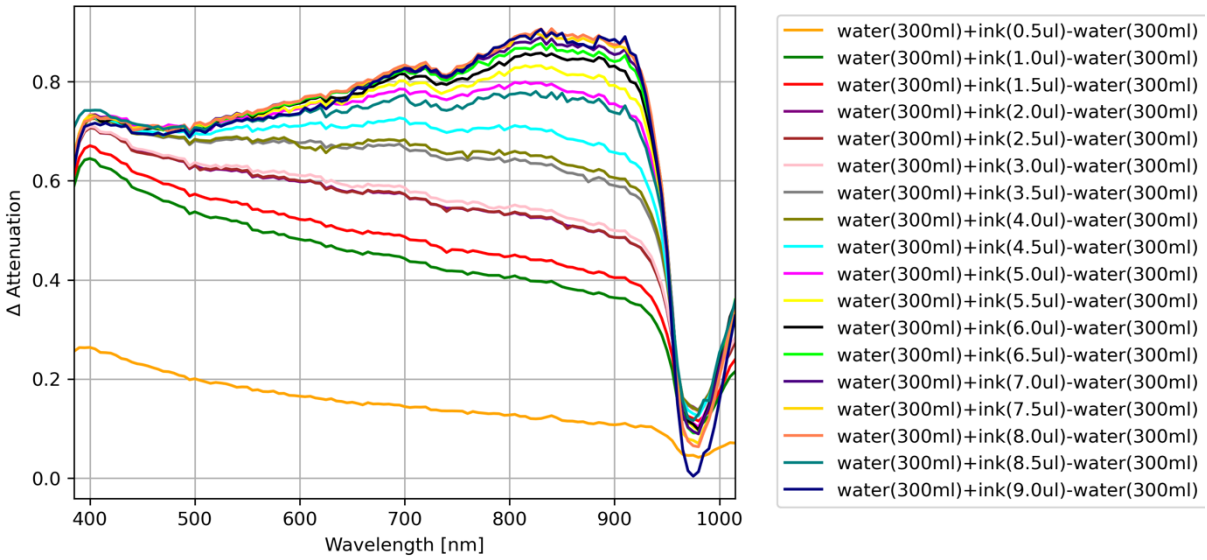

Figure 8. Delta attenuation spectra of the Phantom W+INK at its various iterations from the data collected and processed from HyperProbe1.1.

As described before, the Phantom W+INK tests HyperProbe1.1 in a low-reflectance scenario, characterised by a minimal SNR for the instrumentation. We aimed to quantify such scenario and the corresponding SNR. Mean intensity from the raw data was calculated from each experimental hypercube by averaging across all the spectral bands and was compared to the mean intensity across the full spectrum of the dark hypercube (Figure 9a). SNR in the measurements for the HyperProbe1.1 system was then calculated from the ratio between the mean intensity of the hypercubes and the mean dark intensity (Figure 9b).

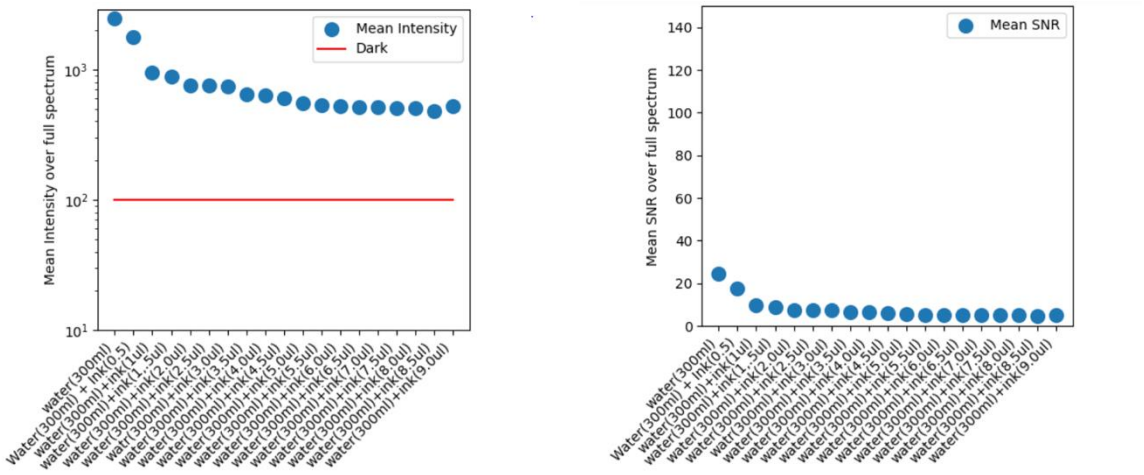

Figure 9. (a) Mean intensity of the raw data from Phantom W+INK averaged across the full working range of HyperProbe1.1, compared with its mean dark intensity (system noise); (b) Mean SNR across the full working range of HyperProbe1.1 from the data collected from Phantom W+INK.

Finally, we also calculated the ratio between the area under each average attenuation spectra in Figure 9a and the total intensity of such spectra across the full working range of HyperProbe1.1. The results of this analysis, shown in Figure 10, depicts a flat, constant trend of such ratio across the various iterations of the Phantom W+INK.

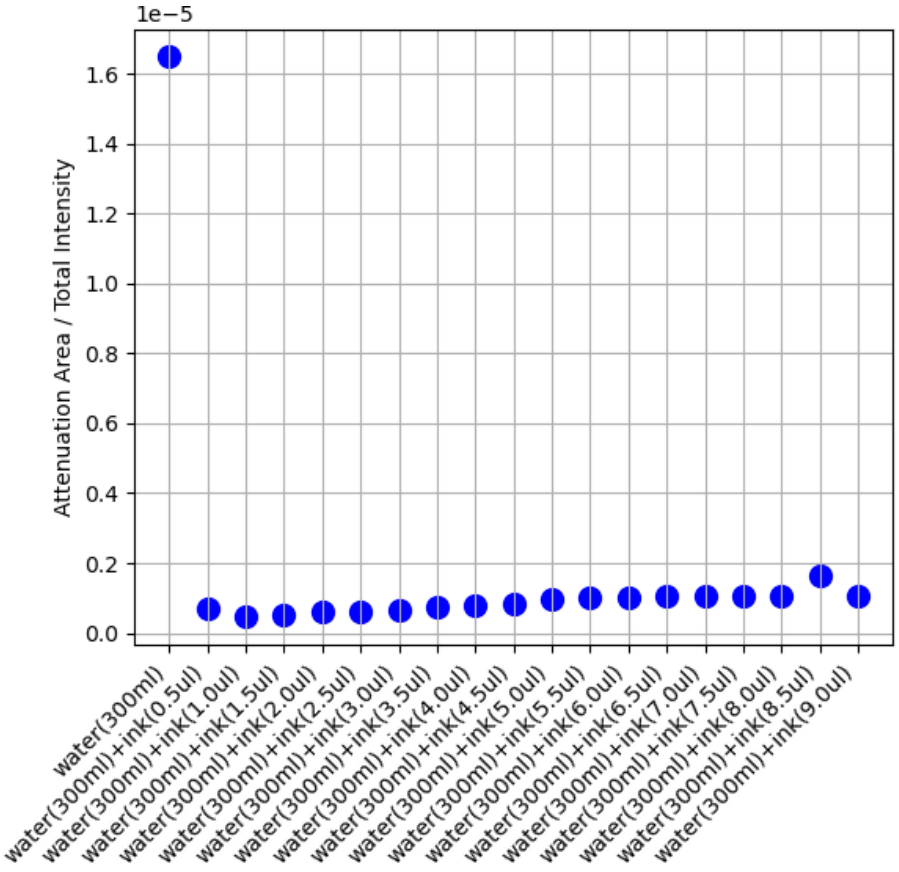

Figure 10.Ratio between the area under the average attenuation spectra for each iteration of the Phantom W+INK and their corresponding total intensity from the data collected with HyperProbe1.1 across its full working range.

Characterisation of HyperProbe1.1 with Phantom W+INK+IL

The same data collection procedures used in the previous section were repeated also for the recipe of Phantom W+INK+IL. This time, exposure time of the HyperProbe1.1 system was set equal to 25 ms (as evidence to the different SNR levels between the recipes). Phantom W+INK+IL introduces tissue-like scattering to the recipe. This was quantified from the composition of the phantom using formulas and methods described in Arnouts et al.[22]. Absorption of fatin the Intralipid solution was also theoretically quantified using absorption coefficients available in literature[23]. Figure 11 reports both the experimental spectra of attenuation collected with HyperProbe1.1, as well as the theoretical spectra of the absorption and scattering coefficients of the Phantom W+INK+IL.

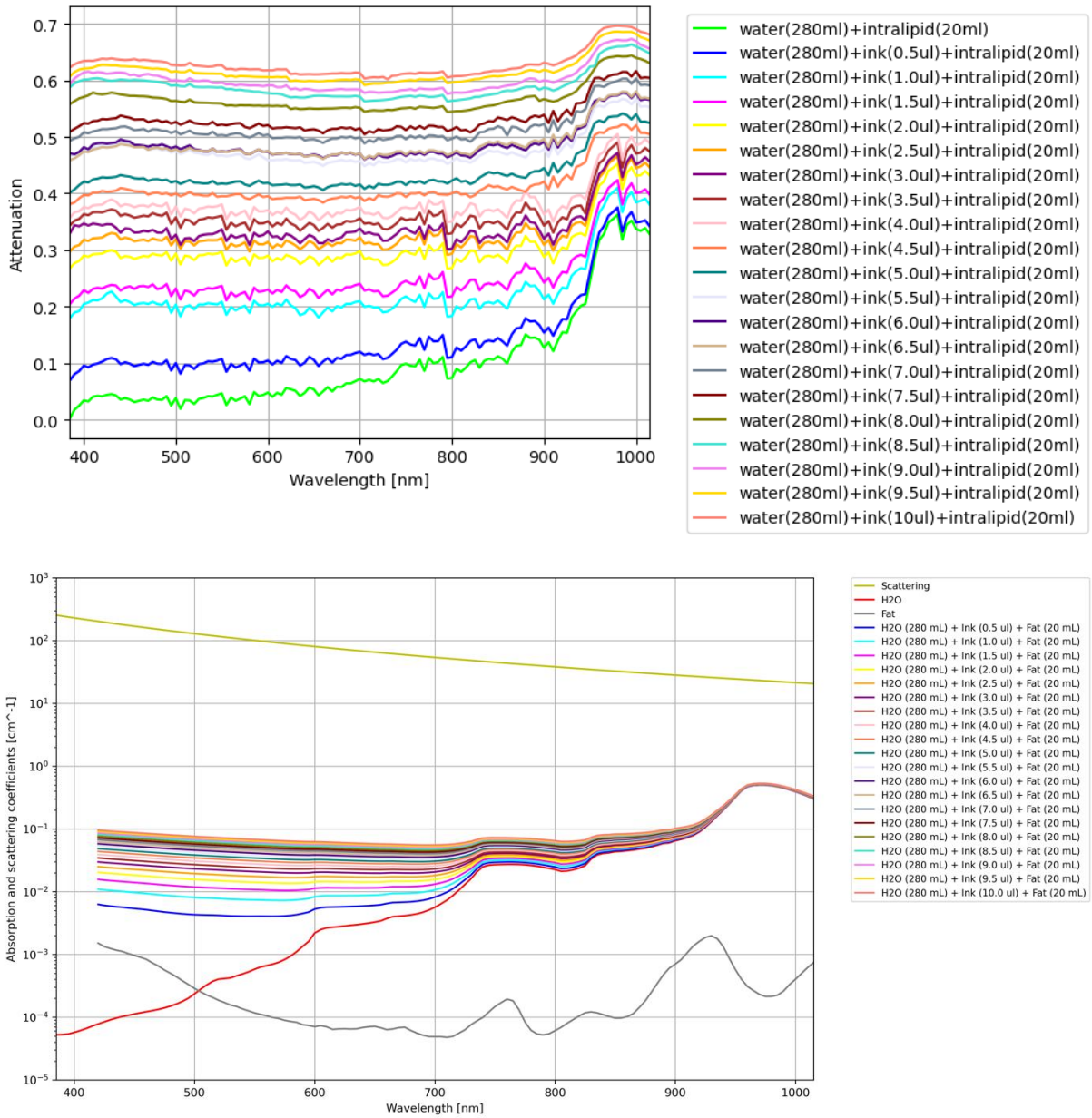

Figure 11.(a) Experimental attenuation spectra of the Phantom W+INK+IL at its various iterations collected and processed from HyperProbe1.1; (b) Theoretical absorption and scattering properties of the Phantom W+INK+IL at its various iterations.

Comparison between experimental and theoretical datasets again demonstrates visible correlation in the spectral trends between the various spectra, demonstrating the capability of HyperProbe1.1 to accurately reconstruct the optical signatures of the target.

Differences in attenuation between the various iteration of the Phantom W+INK+IL and a reference phantom containing only water and intralipid (pure scattering with no ink absorption) were also calculated in terms of Δ attenuation, again across all the different wavelengths from 385 to 1015 nm., as depicted in Figure 12.

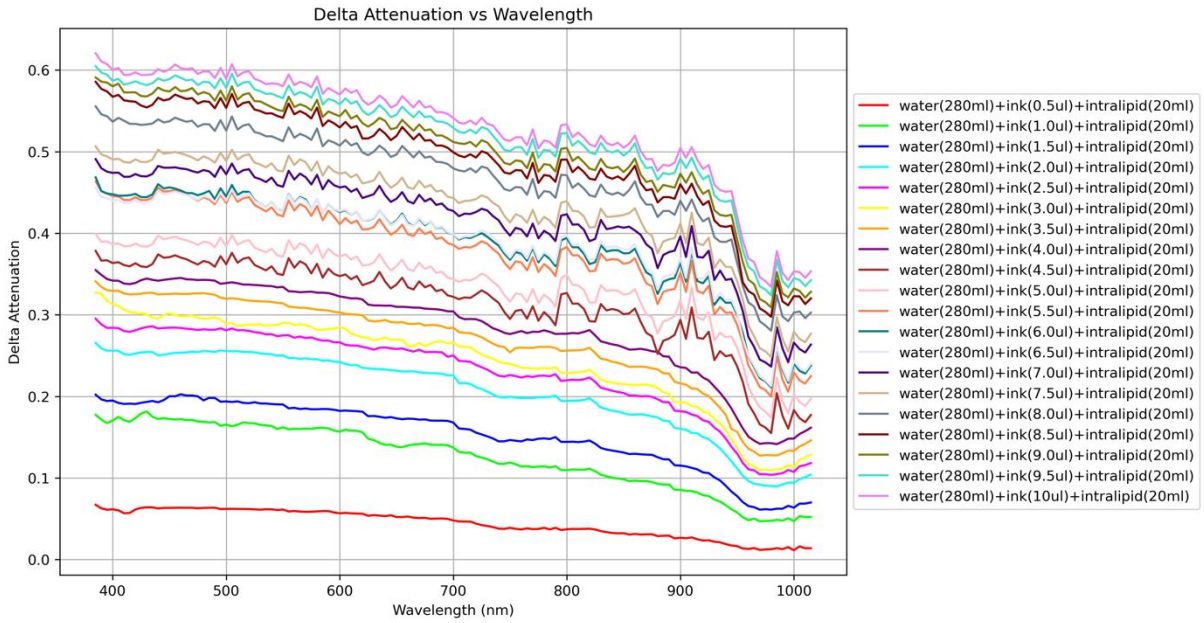

Figure 12.Delta attenuation spectra of the Phantom W+INK+IL at its various iterations from the data collected and processed from HyperProbe1.1.

As for the previous recipe, quantification of mean intensity in the raw spectral data from Phantom W+INK+IL vs. average dark noise of HyperProbe1.1, as well as of average SNR in the measurements, were performed and the results of this are shown in Figure 13.

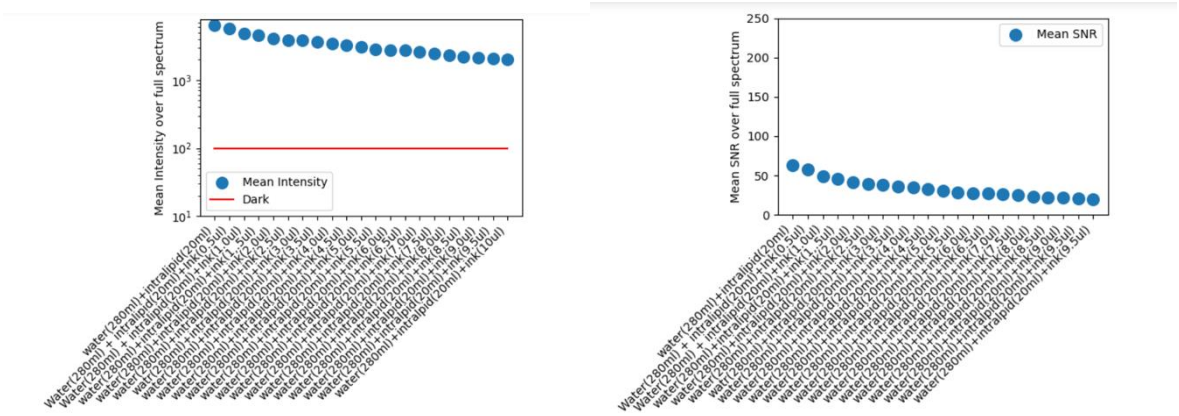

Figure 13. (a) Mean intensity of the raw data from Phantom W+INK+IL averaged across the full working range of HyperProbe1.1, compared with its mean dark intensity (system noise); (b) Mean SNR across the full working range of HyperProbe1.1 from the data collected from Phantom W+INK+IL.

Finally, we again calculated the ratio between the areas under the curve of each experimental attenuation spectra obtained with HyperProbe1.1 and their corresponding total intensity for the datasets collected for the various iterations in Phantom W+INK+IL (Figure 14). Compared to the results from Phantom W+INK in Figure 10, for the outcomes of the testing of HyperProbe1.1 on Phantom W+INK+IL we obtained a linearly increasing trend in the calculated ratio for increasing values of ink absorption.

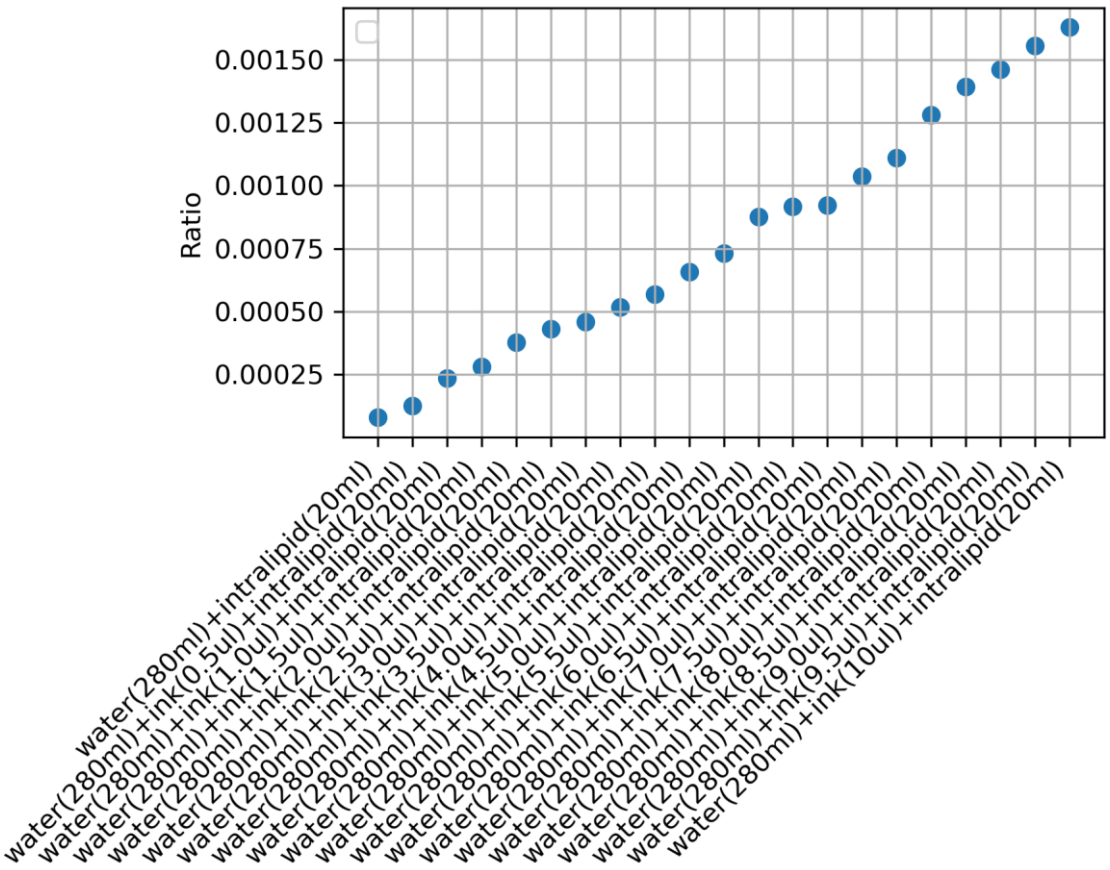

Figure 14. Ratio between the area under the average attenuation spectra for each iteration of the Phantom W+INK+IL and their corresponding total intensity from the data collected with HyperProbe1.1 across its full working range.

3.2. Phantom recipes for the assessment of specific biological contrasts

Both UCL hand UCBL had previously developed phantom recipes to assess the reflectance and fluorescence contrasts of interest[24,25]. In the context of HyperProbe, the main challenge will be to perform both measurements of reflectance and fluorescence on the same phantom.

The basic components of the phantoms are similar for both the reflectance and fluorescence phantoms. They are based on a Phosphate-buffered saline (PBS) buffer, Intralipid 20% (to induce the scattering), and blood (to induce the oxygenation contrast). For the metabolism contrast, yeast can be added to the phantom to add cytochromes.

The basic principles of these phantoms are that the blood will provide the haemoglobin which will provide the oxygenation contrast. Once, the blood is added, its oxygenated state can be set to 100% by bubbling O_2 in the solution. This will result in the haemoglobin to be fully oxygenated. Then, one can induce a deoxygenation of the solution by bubbling N_2 in the solution. N_2 washes-out O_2 in a diffusion process and consequently reduces the blood's oxygenation. Thus, by alternatively bubbling O_2 and N_2 in the solution, one can control the oxygenation contrast in the solution. Alternatively, when using yeast, no N_2 is needed. Indeed, the yeast will consume the oxygen in the solution and reduce the blood's oxygenation. Additionally, as the oxygen level drops, the oxidative state of the cytochromes in the yeast will change, providing the metabolic contrast. Thus, these blood/lipids phantom provide a way to test the oxygenation and metabolic contrast of the system developed. Moreover, by evaluating the deoxygenation with and without yeast, one can assess the absence of crosstalk between the metabolic and oxygenation contrast. An example of these kind of phantoms can be found

on figure 15, that shows the typical contrast retrieved with two NIRS systems (a time-resolved NIRS system[24], and a broadband continuous wave (CW) system[26]) with and without yeast. The left and right columns report the results of the yeast and N_2 phantoms respectively. The first line reports the changes in [HHb] and [HbO_2] for both instruments, and the second line reports the changes in [oxCCO] for both instruments. We see that the results are very similar between the two instruments. For the yeast phantom, the two cycles of deoxygenation are similar in terms of values and dynamic. We note an increase in [HHb] together with a decrease in [HbO_2] and [oxCCO]. For the N_2 phantom, [HHb] and [HbO_2] are similar to the yeast phantom. Note that only one cycle of deoxygenation was performed here as the deoxygenation time was longer that with the yeast. In terms of [oxCCO], we see that there is no significant variation during the course of the experiment, as no yeast is present in the solution. The comparison between the yeast and N_2 phantoms validates the capability of the system to detect [oxCCO]. Indeed, by taking the N_2 phantom as a reference for invariant [oxCCO], we can confirm that the [oxCCO] variation detected in the yeast phantom is not due to crosstalk.

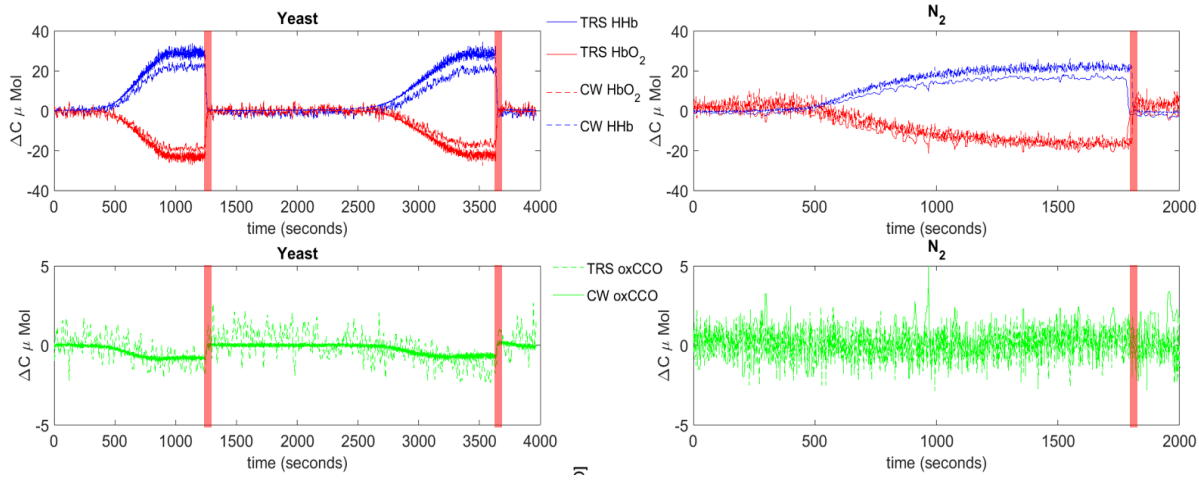

Figure 15. Typical oxygenation and metabolism contrast in blood/lipid phantom. From top to bottom - Concentration changes in [HHb] and [HbO_2] for both the TR and CW instrument, Concentration changes in [oxCCO] for both the TR and CW instrument. Left and right columns refer to yeast and N_2 phantom respectively. Extracted from [24].

The Fluorescence phantoms are similar in terms of composition, with on top of the addition of commercial PpIX to induce the fluorescence contrast. Figure 16 shows an example of the typical fluorescence spectra of the PpIX, and the effect of the detected intensity of the PpIX fluorescence when the blood content of the phantom is varied with the UCBL system[25]. One can note the effect on the blood concentration on the fluorescence peak.

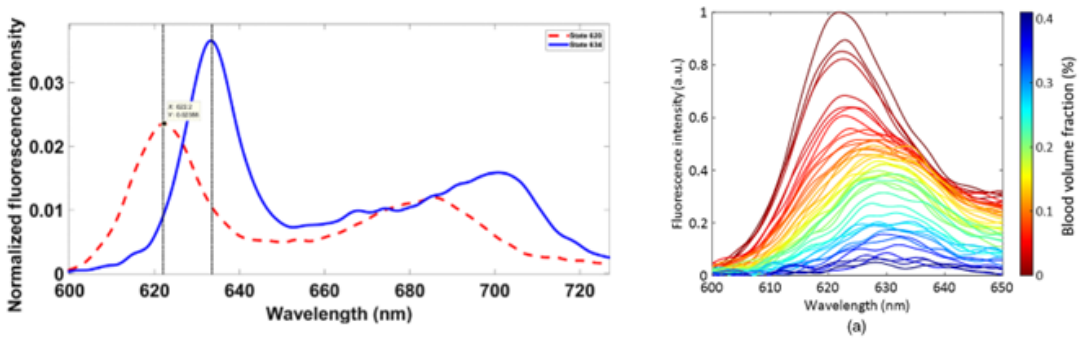

Figure 16. (a) Fluorescence emission spectra of the two states of PpIX considered as reference spectra, normalized by their total intensity. (b) PpIx fluorescence intensity as function as blood content. Extracted from [25].

As seen above, the base components needed to produce the phantoms are well characterized in each mode. However, the specific interaction of the fluorescence compounds on the reflectance mode had not been assed. Moreover, the UCL team had been using human blood for their experiment, whereas UCBL had been using animal blood. Therefore, here we wanted (i) to assess whether human and animal blood can be used indifferently and (ii) to evaluate the effect of the PpIX on the reflectance spectra of these phantoms.

To do so, we have (i) evaluated the same phantom with two types of blood, i.e., defibrinated horse blood that can be easily purchased from a chemical supplier (https://uk.vwr.com/store/product/9131472/animal-blood-serum-products-for-microbiology) and expired human red blood cells that are typically used at UCL, and (ii) assessed individually the effect of the PpIX on the reflectance spectra compared to the baseline solution, composed of PBS and Intralipid, and then the effect of PpIX when blood is added and its oxygenation varied. We will report these evaluations (performed at UCL) below.

A – Comparison between human and horse blood

In order to compare the differences between the human and the horse blood, we first compared their absorption spectra using a commercial spectrophotometer (PerkinElmer Lambda 750 S). We first prepared a solution of 5% blood in PBS for both blood type. Then the blood samples where fully oxygenated by bubbling O_2, and by monitoring the level of dissolved oxygen (DO_2) in these solutions. Once fully oxygenated, the absorbance of the solution was measured in the spectrophotometer in the range 400:5:850nm.

A second sample of deoxygenated blood was measured in the same condition. In order to induce the deoxygenation of the solution, a small quantity of sodium dithionite was added to the oxygenated solution, and the measurement was taken after the DO_2 meter reading had fallen to 0%. Figure 17 reports the spectra of the oxygenated and deoxygenated blood for the human and horse blood.

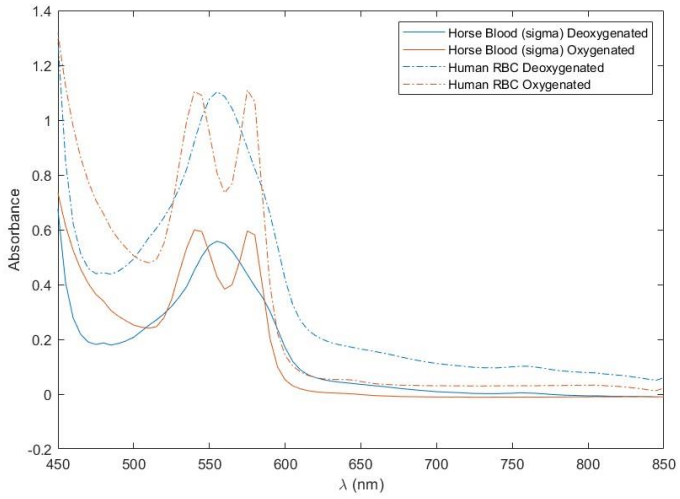

Figure 17. Absorbance spectra measured in the commercial spectrophotometer for both human and animal blood.

One can see that the spectral shape of both bloods, both in the oxygenated and deoxygenated state are identical, displaying the spectral signature of the oxygenated and deoxygenated haemoglobin. One can also note that the absolute absorbance values of the human blood used are higher than the horse blood. This comes from the fact the human blood used here is expired red blood cells and not whole blood, like the horse one. Thus, the absolute concentration of haemoglobin for the same amount of liquid is higher for the human blood.

In order to compare the two blood types in a typical phantom, we also performed a measurement with our standard recipe, i.e., with scattering in a reflectance mode. The setup used to test the different components was a metallic container, of dimensions 27 × 15 × 16 cm. The sides and bottom of the container were coated with a matt black absorbing paint to prevent any reflections from the boundaries. To ensure precise measurements of the volume, particularly for the large volumes of basal solution required, a gravimetric approach was used, as weighing liquids is a valid and accurate method for determining volume. DO_2 levels within the solutions were monitored using a calibrated oxygen probe. Solution pH was concurrently monitored using a pH probe. The entire setup was placed on a hot stirring plate complete with a temperature probe, set to maintain a constant 37°C. Constant stirring at 700 RPM ensured that the solution remained homogeneous.

The optical setup was composed of a broadband light (HL-2000 UV-Vis-NIR Halogen Light Source by Ocean Optics) for the source and of a USB4000 spectrometer (Ocean Optics) for the detection. Light was guided from the light source and to the spectrometer via optical fibres with s source detector distance of 1 cm. A picture of the entire setup can be found on figure 18

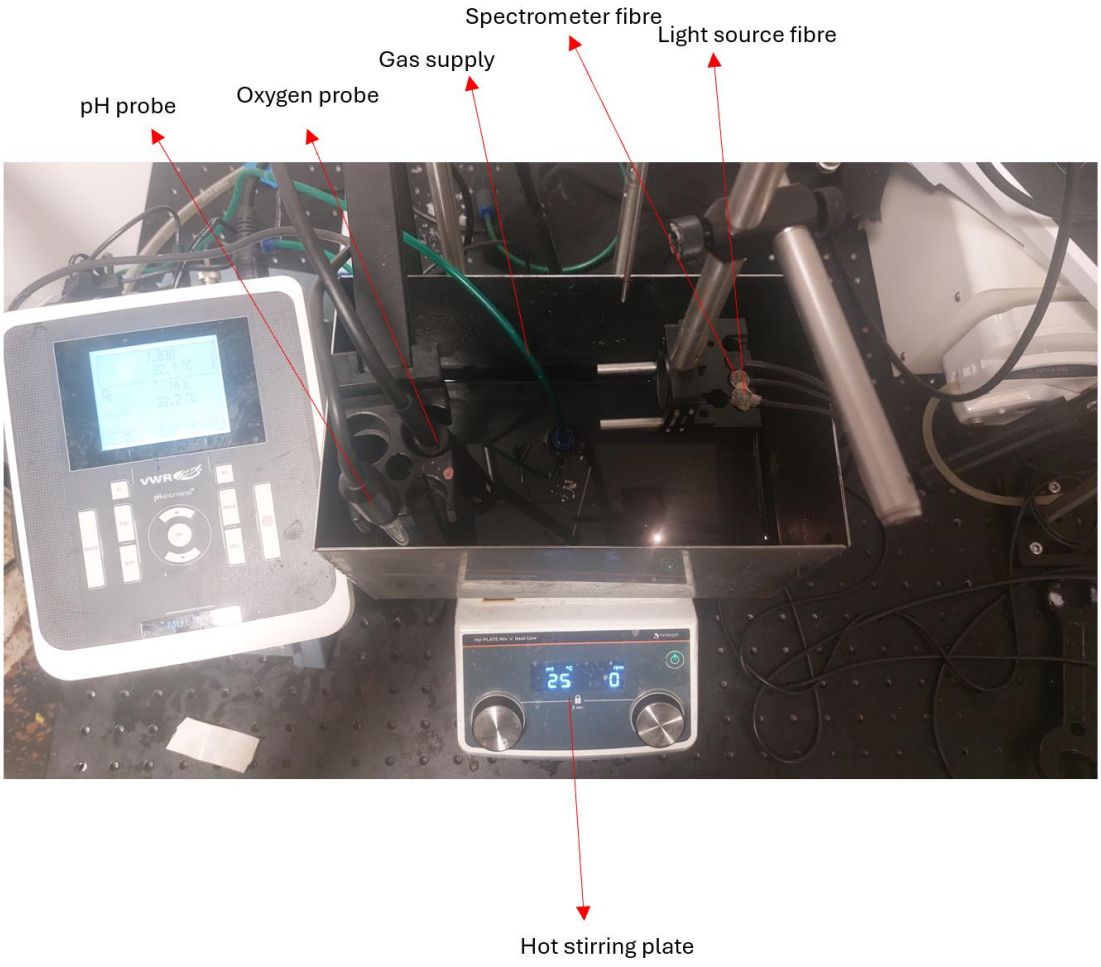

Figure 18. Typical measurement setup.

The compositions of the baseline solution for the two phantoms is of 1400g of PBS solution (at 50mM) and 75g of Intralipid 20%. Then 5 mL of blood were added to the phantom. The oxygenation values of the blood were then varies using N_2.

Figure 19 presents the comparison between the human and horse blood spectra for the difference in absorbance between the fully oxygenated and fully deoxygenated state in the NIR. This region was chosen because of the better sensitivity of our spectrometer to this region and the fact that this is the typical spectral region that the UCL team uses to evaluate haemoglobin concentration.

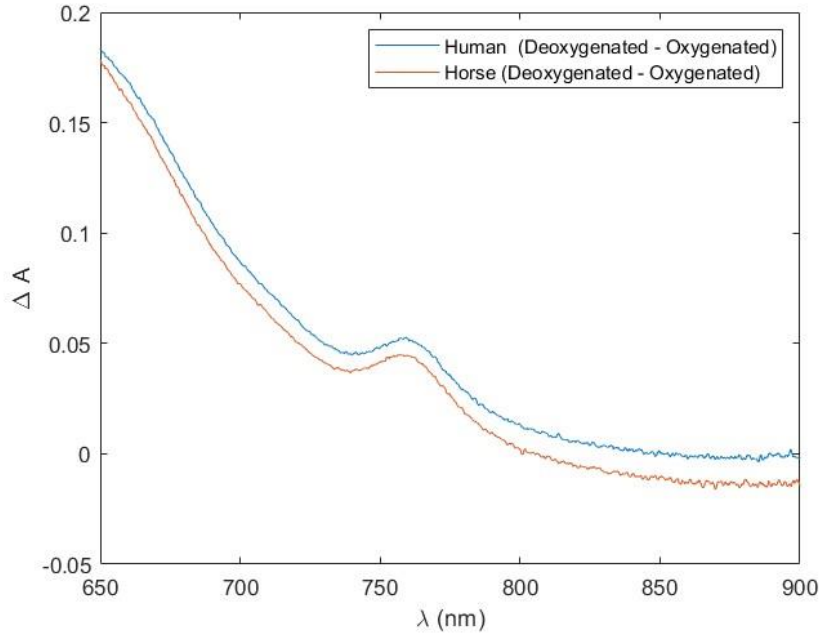

Figure 19. Difference spectra measured in the standard phantom for both animal and human blood.

As for the spectrophotometer measurements, we can see that the spectral shape is identical, with an offset between the human and horse blood, which is essentially associated to the difference in actual haemoglobin concentration between the two samples.

The very similar spectral characteristics of both blood types both measured in transmittance in a non-scattering media and in reflectance in a scattering environment allows us to conclude that there should not be any significant difference in the behaviour of different blood in our phantom and that we can thus use them indifferently in our phantom recipes.

B - Validation of the absence of crosstalk between the reflectance and fluorescence measurements

In order to evaluate the effect of PpIX on our reflectance spectra, we first characterized its absorbance in the commercial spectrometer, as for the blood. To do so, we prepared a solution of 1.2mM of PpIX in dimethyl sulfoxide (DMSO), to reproduce what was done in the recipe from UCBL[25]. The absorbance of PpIX can be found in figure 20. We can see five main peaks of PpIX absorption at 408, 510, 540, 565 and 630 nm, and no particular absorption peak in the NIR above 650 nm.

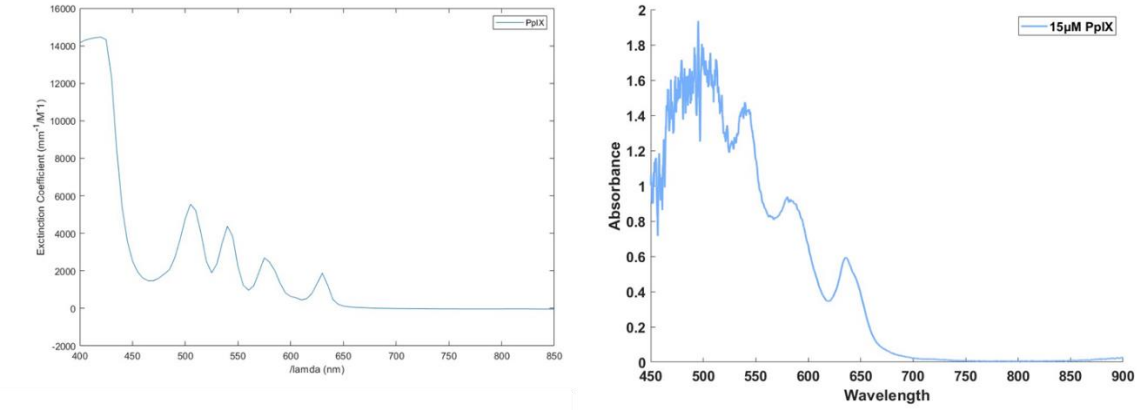

Figure 20. Absorbance of PpIX. (a). As measured in the spectrophotometer for a concentration of 1.2mM (b). Measured in the standard phantom with only IL, for a PpIX concentration of 15 uM.

Similarly to the blood investigation, we explored the effect of the PpIX in our typical measurement, i.e., in a reflectance mode in a diffusive media with the same setup as described in section 3.2.A. We retrieve the same behaviour in the intralipid, with the same absorption peak, as seen on figure 20. One should note that the SNR of instrument is not sufficient to go below 450nm.

We them investigated if the presence of PpIX would influence the reflectance of our blood phantoms. To do so, we reproduce the same recipe as described in section 3.2.A and compared the results of a deoxygenation cycle with and without PpIX. To do so, we started with the same baseline solution of blood/IL/PBS and induced a deoxygenation with N_2, then we added PpIX in the solution to reach a concentration of 15uM, as in reference [25]. We then reoxygenated the solution and induced another deoxygenation with N_2.

Figure 21 shows the comparison of the oxygenated and deoxygenated spectra both with and without PpIX. We can see that the addition of PpIX results in the presence of its typical absorption peaks both in the oxygenated and deoxygenated state of the blood.

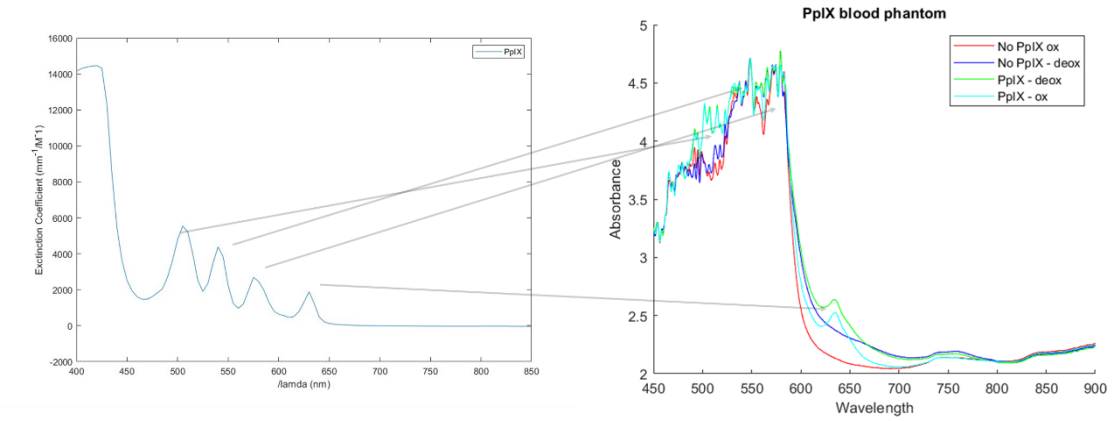

Figure 21. (a) typical PpIX absorbance spectrum (b) Spectra of a typical phantom containing water + IL + Blood + PpIX. One can note that we retrieve the typical absorption peaks of the PpIX.

Finally, we compared the deoxygenation time dynamic between before and after the addition of PpIX. To do so, we calculated the concentration change in [HHb] and [HBO_2] between the start and the end of the N_2 bubbling that induces the deoxygenation. The calculation was done using the modified beer lambert-law (MBLL) in the range 790 to 870 nm. This wavelength range was used as it is the typical wavelength range that we use in the NIR to evaluate these

species. Moreover, in this range, the contribution of PpIX is minimal and thus no particular crosstalk is expected. Figure 22 reports the results of the change [HHb] and [HBO_2] both with and without PpIX.

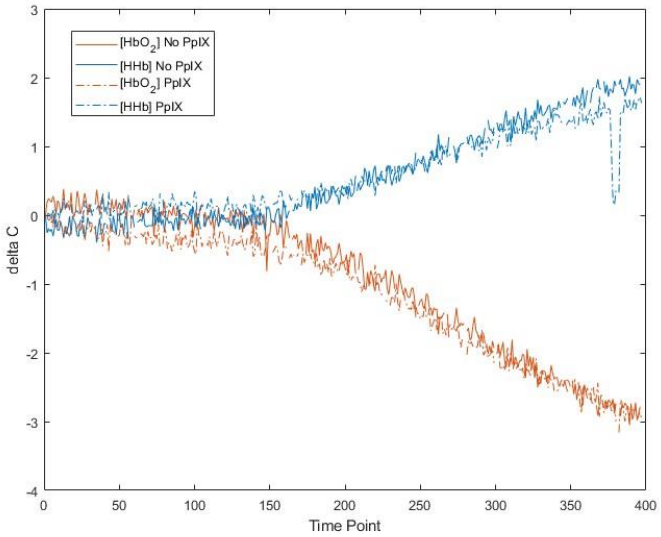

Figure 22. Time dynamic of the oxygenation change in the same phantom before and after the addition of PpIX.

We can see that the time dynamic and magnitude of the concentration changes are very similar with or without PpIX. Thus, we can conclude that there is no significant effect of PpIX on the blood deoxygenation and that it will not change our reflectance-based contrast. However, we can note that the wavelength range used here cover a window where PpIX does not have any significant absorption peak. Therefore, more work still needs to be done in order to assess the effect of the absorption spectra of PpIX on the fit of the concentration of haemoglobin, especially in the visible range. Similarly to our N_2 versus yeast phantom, the potential crosstalk between PpIX and haemoglobin can be evaluated by comparing a phantom with and without PpIX. However, this evaluation was out of the scope of this deliverable and we will investigate this effect in the future.

C – Investigation on yeast fluorescence

On top of the PpIX fluorescence signal, we are considering the possibility of also assessing the NADH and FAD contrast with our HyperProbe system. We would then need a compound to induce this kind of contrast in our phantoms. We thus explored the possibility of using commercial yeast to induce this kind of contrast. To do so, we characterised yeast autofluorescence at UNIFI using a commercial luminescence spectrometer (PerkinElmer LS 55). The LS 55 uses a Xenon lamp excitation at multiple, selectable bands between 300 and 800 nm, and a Monk-Gillieson type monochromator equipped with low stray light, holographic gratings that can acquire broadband fluorescence in the range 200-800 nm with zero order selectable.

For the characterisation, a solution of water and commercial baker's yeast (*Saccharomyces cerevisiae*) diluted at a concentration of 20 mg/mL was inserted in a 10-mm squared Polystyrene (PS) cuvette and analysed in the luminescence spectrometer, by illuminating it in sequence from 300 to 700 nm at 20-nm steps. Full fluorescence spectra were acquired at each iteration from a starting wavelength equal to the illuminating one plus 20 nm to the end of the working range (900 nm). Reference fluorescence spectra accounting from water and PS contribution were also acquired with the cuvette without any yeast, illuminated from 300 to 400

nm at 20-nm steps. Raw results of all these fluorescence measurements are reported in Figure 23.

The raw results are characterised by artifacts related to second-order effects, visible in the predominant shifting peaks in almost all the spectra (according to range) at central wavelengths approximately corresponding to twice the value of the respective excitation wavelengths. Influences from back-scattering and reflection of the illumination light are also present at the left edges of the spectra. Therefore, analysis on the spectra was done by eliminating the intervals of the range were the second-order peaks were present (Figure 24), with localisation of the fluorescence features of interest reported as central wavelengths of Gaussian fittings of the main peaks. These were then correlated to known fluorescence fingerprints of fluorophores present in yeast from literature in a range of interest up to 740 nm[19].

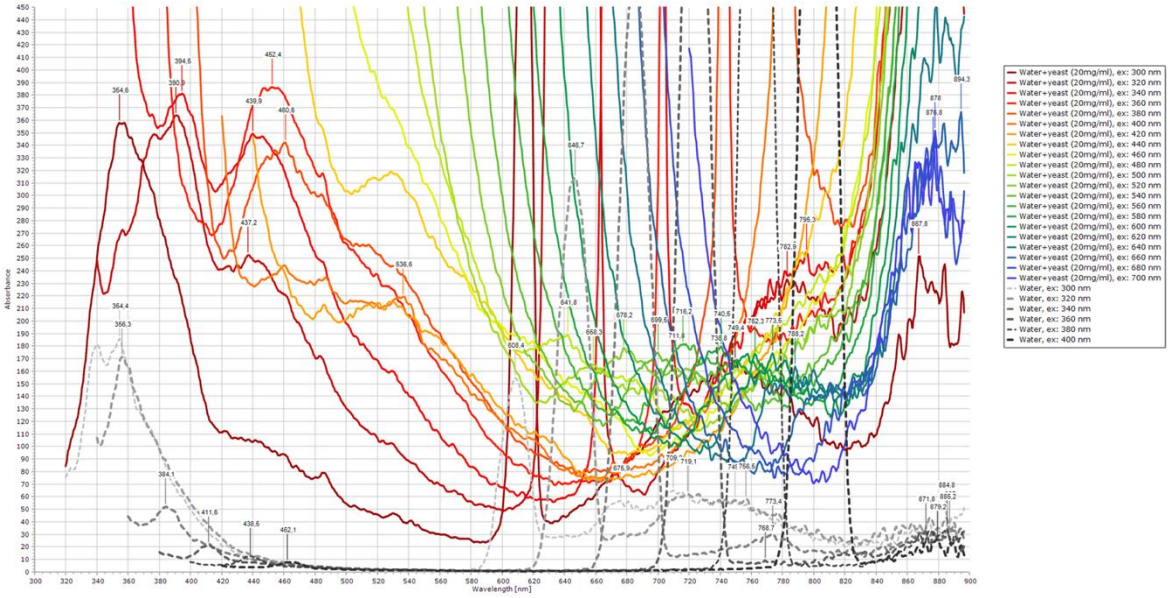

Figure 23. Fluorescence spectra of a solution of water and yeast in a PS cuvette experimentally measured with a commercial luminescence spectrometer at different excitation wavelengths (solid lines). The dashed lines report the reference spectra for the measurements of only the cuvette with water.

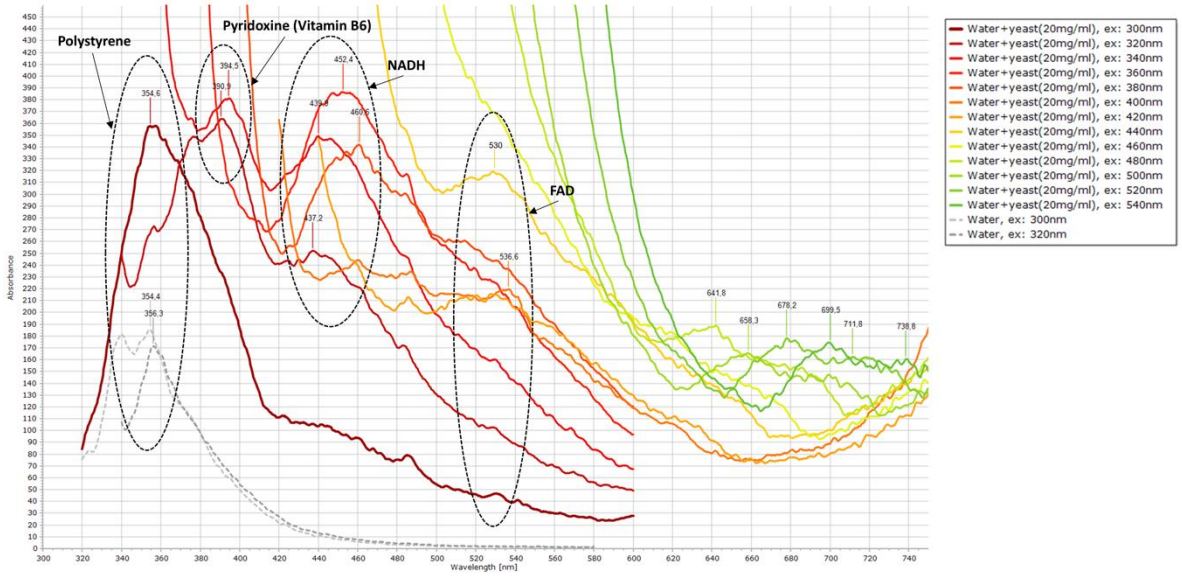

Figure 24. Corrected fluorescence spectra of a solution of water and yeast in a PS cuvette with identification of features corresponding to known signatures of fluorophores present in the yeast, in particular autofluorescence of FAD and NADH.

From the comparison between the yeast fluorescence spectra for illuminations at 300 and 320 nm with the corresponding references for only water and the PS cuvette, a first feature peak at about 355 nm can be identified and correlated to fluorescence contamination from PS (as this is present also in the reference spectra). Among the known fluorophores present in yeast, from the results we can also identify features from pyridoxine (a form of Vitamin B6) at about 390-395 nm, albeit this has no known role as biomarker of interest for our purposes. Finally, from the fluorescence characterisation of the yeast we demonstrate the presence of autofluorescence from NADH and FAD (as reported in Section 2.2) with peaks ranging at about 435 to 460 nm, and at about 530-535 nm, respectively. Beyond 600 nm, a number of minor peaks have been identified, which we could hypothesise may belong to different species of porphyrins, yet it is not possible to discriminate them accurately enough. Thus, from these initial results, we can note that the yeast could be a viable solution to mimic the NADH and FAD fluorescence in our phantom.

D – Recipes summary

We have presented here the main compounds that can be used to mimic the contrast of interest that we will investigate *in vivo* with our HyperProbe systems. In the reflectance measurements, the contrasts are detected by assessing change in the absorption between the oxygenated and deoxygenated states. The main fluorescent contrast of interest is the PpIX, which can be easily added to the solution. Its interaction with our reflectance measurement have been characterized and we could see that the presence of PpIX did not affect the detection of our contrast in the NIR range. However, we have seen that the typical peaks in the visible of the PPIX where present and that their effect will need to be taken into account when this wavelength range is used for quantification.

For the fluorescence, on top of the PpIX contrast, we could also explore the NADH and FAD contrast. However, the exploration of this contrast will also depend on the capacity of our final instrument. A limiting factor for this contrast is the use of an illumination wavelength in the UV which could introduce various complexities. In this eventuality, we have started exploring the possibility to use yeast to induce these fluorescent signals, and our initial results show that it

could be a viable agent to mimic them. However, more work still remains to be done to precisely characterise the use of yeast to induce NADH and FAD signals.

We thus have liquid phantom recipes that can mimic our current main contrast of interest. Table 4 summarizes the compounds of the phantom needed to induce each type of contrast with the typical volume fraction needed to mimic realistic *in-vivo* values.

Table 4. Summary of the phantom recipes.

Contrast	Compounds	Typical quantities	Notes
NA (Baseline)	PBS + water	Baseline compounds that will be at least 97% of the total volume of the phantom	This is the baseline components of any phantom.
Scattering	IL	5% of volume to get typical scattering properties of tissues	Can scale scattering properties based on IL concentration. Note that the Intralipid
Oxygenation	Blood	Typically, between 0.1 and 2% to get typical haemoglobin concentration of tissues.	Animal or human blood can be used indifferently.
Metabolism	yeast	Typically, between 0.1 and 1% of volume to get typical cytochrome contrast.	In order to test the crosstalk between the cytochromes and the other contrast, the basic strategy will be to do measurement with and without yeast.
PpIX	PpIX	Typically, between 0.1 and 1% of volume to get typical PpIX concentration.	In order to test the crosstalk between the PpIX and the other contrast, the basic strategy will be to do measurement with and without PpIX.
NADH and FAD	yeast	Not precisely characterised yet	Our initial results indicates that yeast could be a suitable agent to mimic the NADH and FAD contrast. However, more work needs to be done to fully characterize this contrast.

4. Discussions and conclusions

In this report, we have described the rational of the phantoms that we have developed here that were aiming at (i) assessing the basic instrument capabilities in terms of signal-to-noise ratio (SNR) and dynamic range, in response to changes in the optical properties of the tissues (i.e. absorption μ_a and reduced scattering μ'_s) and (ii) assessing the capacity of the systems to detect specific biochemical contrast of interest. The first goal was achieved by using well known phantom recipes based on Indian ink and Intralipid, allowing us to control the optical properties of the solution to assess the basic responses of the system in response to specific optical properties.

For the second goal, we based our recipes on previous work undergone at UCL and UCBL to produce phantoms with contrast focused on reflectance or fluorescence. These phantoms are based on a PBS/water/lipid solution (to induce the scattering), blood (for the oxygenation contrast), yeast (for the metabolic contrast), and PpIX (for the fluorescence contrast). The main validation work performed here consisted in evaluating the effect of the blood used, and of the

effect of the PpIX on the reflectance signals. Indeed, the UCL and UCBL team had used human and animal blood respectively in their recipes. Thus, we wanted to compare the results on the same phantom between the human blood typically used at UCL, and animal blood commercially available. Our results showed that there was no significant difference between these two blood types and thus that the commercially available blood could be used in the phantom recipes. As only UCL has access to human blood, this will largely facilitate the use of the phantom in any of the partners facilities. The second evaluation that we did was to test the effect the PpIX on our reflectance spectra. Indeed, the UCBL team had already used similar recipes to assess the fluorescence. However, the effect of the PpIX on the reflectance spectrum had not been evaluated. As we aim to develop a system that monitor both the reflectance and fluorescence signals, we needed to confirm that the fluorescence agent would not have an effect on our reflectance monitoring. We could confirm that the PpIX does not induce any significant effect apart from adding its absorption signature in its typical wavelength range. Thus, we will be able to use PpIX in the phantom to evaluate simultaneously the fluorescence and reflectance contrast.

Finally, it is worth noting that we started evaluating the potential use of yeast as a mimicking agent for NADH and FAD fluorescent contrast. Even though our system does not have the current capacity to evaluate these contrasts, as the illumination wavelength need to be in the UV, we are considering this addition to improve even more the capacity of our instrument. We will thus continue to work on the possibility of using yeast to mimic these contrasts, as we could acquire promising initial results, but precise characterisation still remains to be done in order to use it efficiently.

To conclude, the recipes to evaluate the detection of these various contrast, and evaluate the potential crosstalk induce by the instrumentation or the algorithms, are now available to all the partners and the team at UNIFI has started the characterisation of the HyperProbe1.1 system with them, notably for the basic instrument capabilities. The next deliverable of this WP will focus on the build of an anatomically accurate phantoms. We plan to base these new phantoms on the recipes that we have developed here. Briefly, by building phantoms with different compartment, and filled with different mixture (for example with and without PpIX), we will be able to assess the spatial accuracy of the contrast estimation with the HyperProbe systems. One of the challenges of building/processing the data of such phantom, is to characterise properly the pathlength of light in this phantom. In order to do this, we will use the instrument simulator and digital phantom developed in task 3.1 to accurately simulate the propagation of the light in it and gain this information.

Data Repository

The datasets of the phantom characterization used for the calibration of the simple liquid phantoms have been made publicly available on Zenodo, at the following link: https://doi.org/10.5281/zenodo.13842471

References

[1] Pogue, B. W. and Patterson, M., “Review of tissue simulating phantoms for optical spectroscopy, imaging and dosimetry.,” J. Biomed. Opt. **11**(4), 41102 (2006).

[2] Jacques, S. L., “Optical Properties of Biological Tissues: A Review,” Phys. Med. Biol. **58**(11), R37-61 (2013).

[3] Kleiser, S., Ostojic, D., Andresen, B., Nasseri, N., Isler, H., Scholkmann, F., Karen, T., Greisen, G. and Wolf, M., “Comparison of tissue oximeters on a liquid phantom with adjustable optical properties: an extension,” Biomed. Opt. Express **9**(1), 86 (2018).

[4] Boas, D., Elwell, C. E., Ferrari, M. and Taga, G., “Twenty years of functional near-infrared spectroscopy: Introduction for the special issue,” Neuroimage **85**, 1–5 (2014).

[5] Im, J. and Rajaram, N., “Optical Molecular Imaging and Spectroscopy of Oxygenation and Metabolism in Tumors,” IEEE J. Sel. Top. Quantum Electron. **22**(3) (2016).

[6] Isler, H., Kleiser, S., Ostojic, D., Scholkmann, F., Karen, T. and Wolf, M., “Liquid Blood Phantoms to Validate NIRS Oximeters: Yeast Versus Nitrogen for Deoxygenation,” [Advances in Experimental Medicine and Biology], 381–385 (2018).

[7] Hyttel-Sorensen, S., Kleiser, S., Wolf, M. and Greisen, G., “Calibration of a prototype NIRS oximeter against two commercial devices on a blood-lipid phantom,” Biomed. Opt. Express **4**(9), 1662 (2013).

[8] Bale, G., Elwell, C. E. and Tachtsidis, I., “From Jöbsis to the present day: a review of clinical near-infrared spectroscopy measurements of cerebral cytochrome-c-oxidase,” J. Biomed. Opt. **21**(9), 091307 (2016).

[9] Rana, R., Huirem, R. S., Kant, R., Chauhan, K., Sharma, S., Yashavarddhan, M. H., Chhabra, S. S., Acharya, R., Kalra, S. K., Gupta, A., Jain, S. and Ganguly, N. K., “Cytochrome C as a potential clinical marker for diagnosis and treatment of glioma,” Front. Oncol. **12**(September), 1–12 (2022).

[10] Lange, F., Dunne, L., Hale, L. and Tachtsidis, I., “MAESTROS: A Multiwavelength Time-Domain NIRS System to Monitor Changes in Oxygenation and Oxidation State of Cytochrome-C-Oxidase,” IEEE J. Sel. Top. Quantum Electron. **25**(1), 1–12 (2019).

[11] Grosenick, D., Rinneberg, H., Cubeddu, R. and Taroni, P., “Review of optical breast imaging and spectroscopy,” J. Biomed. Opt. **21**(9), 091311 (2016).

[12] Ninni, P. Di, Martelli, F. and Zaccanti, G., “Intralipid: towards a diffusive reference standard for optical tissue phantoms.,” Phys. Med. Biol. **56**(2), N21-8 (2011).

[13] Quarto, G., Spinelli, L., Pifferi, A., Torricelli, A., Cubeddu, R., Abbate, F., Balestreri, N., Menna, S., Cassano, E. and Taroni, P., “Estimate of tissue composition in malignant and benign breast lesions by time-domain optical mammography,” Biomed. Opt. Express **5**(10), 3684–3698 (2014).

[14] Su, X., Huang, Q. F., Chen, H. L. and Chen, J., “Fluorescence-guided resection of high-grade gliomas: A systematic review and meta-analysis,” Photodiagnosis Photodyn. Ther. **11**(4), 451–458 (2014).

[15] Herms, J., Stepp, H., Johansson, A., Palte, G. and Schnell, O., “5-Aminolevulinic Acid-induced Protoporphyrin IX Levels in Tissue of Human Malignant Brain Tumors,” 1373–1378 (2010).

[16] Stummer, W., Pichlmeier, U., Meinel, T., Wiestler, O. D., Zanella, F., Reulen, H. and Study, A., “Fluorescence-guided surgery with 5-aminolevulinic acid for resection of malignant glioma : a randomised controlled multicentre phase III trial” (2006).

[17] Marois, M., Bravo, J., Davis, S. C. and Kanick, S. C., “Characterization and standardization of tissue-simulating protoporphyrin IX optical phantoms,” J. Biomed. Opt. **21**(3), 035003 (2016).

[18] Giannoni, L., Lange, F. and Tachtsidis, I., “Hyperspectral imaging solutions for brain tissue metabolic and hemodynamic monitoring: past, current and future developments,” J. Opt. **20**(4), 044009 (2018).

[19] Maslanka, R., Kwolek-Mirek, M. and Zadrag-Tecza, R., “Autofluorescence of yeast Saccharomyces cerevisiae cells caused by glucose metabolism products and its

methodological implications," J. Microbiol. Methods **146**(January), 55–60 (2018).

[20] Durduran, T., Choe, R., Baker, W. B. and Yodh, a G., "Diffuse optics for tissue monitoring and tomography," Reports Prog. Phys. **73**(7), 076701 (2010).

[21] Spinelli, L., Botwicz, M., Zolek, N., Kacprzak, M., Milej, D., Sawosz, P., Liebert, A., Weigel, U., Durduran, T., Foschum, F., Kienle, A., Baribeau, F., Leclair, S., Bouchard, J.-P., Noiseux, I., Gallant, P., Mermut, O., Farina, A., Pifferi, A., et al., "Determination of reference values for optical properties of liquid phantoms based on Intralipid and India ink," Biomed. Opt. Express **5**(7), 2037 (2014).

[22] Aernouts, B., Van Beers, R., Watté, R., Lammertyn, J. and Saeys, W., "Dependent scattering in Intralipid® phantoms in the 600-1850 nm range," Opt. Express **22**(5), 6086 (2014).

[23] Giannoni, L., Lange, F. and Tachtsidis, I., "Investigation of the quantification of hemoglobin and cytochrome-c-oxidase in the exposed cortex with near-infrared hyperspectral imaging: A simulation study," J. Biomed. Opt. **25**(4) (2020).

[24] Lange, F., Dunne, L., Hale, L. and Tachtsidis, I., "MAESTROS: A Multiwavelength Time-Domain NIRS System to Monitor Changes in Oxygenation and Oxidation State of Cytochrome-C-Oxidase," IEEE J. Sel. Top. Quantum Electron. **25**(1), 1–12 (2019).

[25] Alston, L., Rousseau, D., Hebert, M. and Mahieu-Williame, L., "Nonlinear relation between concentration and fluorescence emission of protoporphyrin IX in calibrated phantoms," J. Biomed. Opt. **23**(09), 1 (2018).

[26] Bale, G., Mitra, S., Meek, J., Robertson, N. and Tachtsidis, I., "A new broadband near-infrared spectroscopy system for in-vivo measurements of cerebral cytochrome-c-oxidase changes in neonatal brain injury," Biomed. Opt. Express **5**(10), 3450 (2014).